THE PUBLISHING HOUSE
OF THE ROMANIAN ACADEMY

PROCEEDINGS OF THE ROMANIAN ACADEMY, Series A,
Volume 25, Number 4/2024, pp. 347–358
DOI: 10.59277/PRA-SER.A.25.4.11

UNLOCKING THE 3D GEOREFERENCING ACCURACY POTENTIAL OF GÖKTÜRK-1 TRI-STEREO PANCHROMATIC LEVEL 2A IMAGES BY SENSOR-DEPENDENT ORIENTATION MODEL

Gürsu AYTEKİN[1], Hüseyin TOPAN[2]

[1] The Embassy of the Republic of Türkiye, Abu Dhabi, United Arab Emirates
[2] Zonguldak Bülent Ecevit University, Department of Geomatics Engineering, Zonguldak, Türkiye
Corresponding author: Hüseyin TOPAN, E-mail: topan@beun.edu.tr

Abstract. The panchromatic tri-stereo images of Göktürk-1, the first sub-meter optical remote sensing satellite of Türkiye, was assessed with respect to 3D georeferencing accuracy using sensor-dependent orientation model. The investigated panchromatic images were acquired in tri-stereo mode with 50 cm ground sampling distance at nadir-view, covering Zonguldak (Türkiye) test site. The sensor-dependent orientation model developed for the Pléiades 1A/1B/Neo and SPOT 6/7 satellites were preferred since the characteristics of Göktürk-1's imaging geometry was identical with them. Two GCP/ICP sets (50/9 and 44/15) were established by in-field GNSS survey, and adjusted georeferencing accuracy were estimated almost millimetre and ~ ± 50 cm (~ ± 1 GSD) at GCPs and ICPs, respectively. All process was carried out by Geo3o1 tool of GeoEtrim derived in MATLAB environment.

Keywords: Göktürk-1, sensor-dependent orientation, 3D georeferencing accuracy, Zonguldak.

1. INTRODUCTION

Following the Bilsat, Rasat and Göktürk-2 satellites, Göktürk-1 is the first sub-meter optical remote sensing satellite of Türkiye, launched on December 5th, 2016 by the European VEGA launcher from French Guiana. The Göktürk-1 was developed by Telespazio as prime contractor and system integrator with the collaboration of Thales Alenia Space as the constructor, Turkish Aerospace Industries, Aselsan AŞ, TÜBİTAK BİLGEM, Roketsan AŞ and TR Technology as the local industrial partners [1]. The satellite is being operated by Turkish Air Force at the Göktürk Ground Station in Ankara (Türkiye). The essential technical specifications can be found by [2, 3, 4].

Although more than seven years passed over its launching, the number of scientific publications subjecting Göktürk-1 is limited, and most of them were derived from on-orbit commissioning phase. Only two publications, i.e. the system level radiated emission and radiated susceptibility tests reported by [5], and satellite's propulsion subsystem design, integration, test and launch campaign activities reported by [6], subjected the pre-launch analyses. In the commissioning phase, the images were evaluated by their radiometric and geometric characteristics. [2] carried out the radiometric calibration and the image quality assessment with respect to signal-to-noise ratio, modulation transfer function and general image quality equation. [3] handled both horizontal and vertical accuracy of various products levels (L3A, L3B, L4A, L4B) covering five test sites in Türkiye. A similar study carried out by [7] for L2A images covering two test sites in Türkiye. The tests in Rome (Italy) were handled by [4] for estimating height accuracy, by [8] for orthoimage generation and validation, and by [9] regarding the classification for land use/cover. The pansharpening quality was analysed by [10] in Ankara (Türkiye). Their images were also analysed for the pixel and object-based classification performance by [11] in Çaycuma district of Zonguldak (Türkiye) test site. The authors of this article assessed the same images using various kinds of sensor dependent and independent orientation models for estimating the 2D georeferencing accuracy in the Zonguldak test site [12]. Besides, the primary evaluation using the existing GCP/ICP sets were carried out by [13] and [14]. Finally, in the doctoral thesis of the first author, a study was carried out to georeferencing accuracy

assessment of tri-stereo Göktürk-1 satellite images by sensor dependent orientation using a more expanded GCP/ICP sets, and by searching the efficiency of various exterior orientation parameters (EOPs) sets [15].

The novelty of this article is that the Göktürk-1 tri-stereo panchromatic level 2A images were assessed by its sensor dependent orientation model to explore the 3D georeferencing accuracy. The studies run by [3–8, 12] evaluated the images' geospatial performance with a generic model, i.e. Rational Function Model (RFM). Nevertheless, the success of this model depends on the Rational Polynomial Coefficients (RPCs) produced by the sensor dependent orientation model. The advantage of using sensor dependent orientation model is that the highest accuracy can be estimated by this model which is close to the real imaging geometry, and the efficiency orientation parameters on the georeferencing accuracy could be estimated. In this article, for the first time, the sensor-dependent orientation model was used to orient Göktürk-1 images, and its accuracy was assessed.

The layout of this manuscript is as follows. The details of the georeferencing accuracy assessment process by using sensor dependent orientation model were given by Section 2. The implementation made at the Zonguldak test site using Göktürk-1 images was handled in Section 3, the implementation results were included in Section 4 and the conclusion and assessment were included in Section 5.

2. 3D GEOREFERENCING USING SENSOR DEPENDENT ORIENTATION MODEL

The sensor dependent orientation model for Göktürk-1 images is identical for the Pléiades 1A/1B/Neo and SPOT 6/7 images, developed by Airbus [16–18] and originated to the models of SPOT 1-5 [19]. The first experience was gained developing a tool called Geo3o1 as a part of GeoEtrim in MATLAB environment by [20], and successfully applied for SPOT 6 following a modification [21]. This tool has the capable of estimating the georeferencing accuracy by i) direct orientation using raw interior and exterior orientation parameters, ii) pre-adjustment of interior orientation parameters for each image individually and iii) bundle adjustment. The Geo3o1 workflow diagram, modified by the first author to read the metadata file of Göktürk-1, is presented in Fig. 1. The Geo3o1 module is a sub-module written specifically to determine the georeferencing accuracy of stereo/triple satellite images using the sensor-dependent orientation model [15, 20].

According to [16–18] in sensor dependent orientation model, image to ground transformation is following,

$$\vec{\boldsymbol{P}} = \begin{bmatrix} \mathrm{X} \\ \mathrm{Y} \\ \mathrm{Z} \end{bmatrix} = \vec{\boldsymbol{P}}_{\boldsymbol{S}} - m\,\underline{\boldsymbol{R}} \begin{bmatrix} -\tan\psi_y \\ \tan\psi_x \\ -1 \end{bmatrix} \tag{1}$$

where $\vec{\boldsymbol{P}} = [\mathrm{X} \quad \mathrm{Y} \quad \mathrm{Z}]^{\mathrm{T}}$ is the object's position in Cartesian coordinate system, $\vec{\boldsymbol{P}}_{\boldsymbol{S}}$ represents the position vector of satellite's mass center in Cartesian coordinate system, m defines scale, $\underline{\boldsymbol{R}}$ is the rotation matrix derived by normalized quaternions, (ψ_x, ψ_y) shows look angles. Below is the rotation matrix $\underline{\boldsymbol{R}}$ expressed in quaternions.

$$\begin{aligned}
r_{11} &= (Q_0^n)^2 + (Q_1^n)^2 - (Q_2^n)^2 - (Q_3^n)^2 & r_{22} &= (Q_0^n)^2 - (Q_1^n)^2 + (Q_2^n)^2 - (Q_3^n)^2 \\
r_{12} &= 2(Q_1^n Q_2^n - Q_0^n Q_3^n) & r_{23} &= 2(Q_2^n Q_3^n - Q_0^n Q_1^n) \\
r_{13} &= 2(Q_1^n Q_3^n + Q_0^n Q_2^n) & r_{31} &= 2(Q_1^n Q_3^n - Q_0^n Q_2^n) \\
r_{21} &= 2(Q_1^n Q_2^n + Q_0^n Q_3^n) & r_{32} &= 2(Q_2^n Q_3^n - Q_0^n Q_1^n) \\
& & r_{33} &= (Q_0^n)^2 - (Q_1^n)^2 - (Q_2^n)^2 + (Q_3^n)^2
\end{aligned} \tag{2}$$

where

$$Q_j^n = \frac{Q_j}{\sqrt{\underline{Q}^{\mathrm{T}}\underline{Q}}}, \quad j = 0,1,2,3 \quad \underline{Q} = [Q_0\ Q_1\ Q_2\ Q_3]^{\mathrm{T}}, \tag{3}$$

$$Q_j = \sum_{i=0}^{3} (Q_j)_i \, t_{\mathrm{CN}}^i \tag{4}$$

The centred normalized time value is calculated as

$$t_{\mathrm{CN}} = \frac{t - t_{\mathrm{offset}}}{t_{\mathrm{scale}}} \tag{5}$$

$$t = t_{\mathrm{ref}} + t_{\mathrm{period}}(x - x_{\mathrm{ref}}) \tag{6}$$

The vector formed by the look angles is calculated by

$$\tan \psi_y = \sum_{i=0}^{n} (\psi_y)_i (y - y_{\mathrm{ref}}) \tag{7}$$

$$\tan \psi_x = \sum_{i=0}^{n} (\psi_x)_i (y - y_{\mathrm{ref}}) \tag{8}$$

where x and y denote the row and column coordinates in image space, respectively.

The equation of image to ground transformation in Eq. (1) can be reformulated in reverse form, from ground to image in adjustment process. The functional model is

$$\begin{aligned} F_{\psi_y} &= \frac{R_{11}^{\mathrm{T}}(X_s - X) + R_{12}^{\mathrm{T}}(Y_s - Y) + R_{13}^{\mathrm{T}}(Z_s - Z)}{R_{31}^{\mathrm{T}}(X_s - X) + R_{32}^{\mathrm{T}}(Y_s - Y) + R_{33}^{\mathrm{T}}(Z_s - Z)} - \tan(\psi_y) = 0 \\ F_{\psi_x} &= \frac{R_{21}^{\mathrm{T}}(X_s - X) + R_{22}^{T}(Y_s - Y) + R_{23}^{\mathrm{T}}(Z_s - Z)}{R_{31}^{\mathrm{T}}(X_s - X) + R_{32}^{\mathrm{T}}(Y_s - Y) + R_{33}^{\mathrm{T}}(Z_s - Z)} + \tan(\psi_x) = 0 \end{aligned} \tag{9}$$

where $\underline{\boldsymbol{R}}^{-1} = \underline{\boldsymbol{R}}^{\mathrm{T}}$ since $\underline{R}$ is an orthogonal matrix. $\vec{\boldsymbol{P}}_{\boldsymbol{S}}$ and its acquisition times, $(Q_j)_i$, t_{offset}, t_{ref}, t_{period}, t_{scale}, x_{ref}, y_{ref}, $\tan(\psi_y)_i$, $\tan(\psi_x)_i$ are directly taken from the Göktürk-1 metadata file. In our functional model, the look angles (ψ_x, ψ_y) are considered observations, t_{offset}, t_{ref}, t_{period}, t_{scale}, coefficients of second order polynomial model for $\vec{\boldsymbol{P}}_{\boldsymbol{S}}$, coefficients of quaternions and approximate coordinates $(X,\ Y,\ Z)$ of check points (ICPs) are assumed parameters to be corrected. The user can choose one or a set of combination of them as adjustment parameters.

The functional model of adjustment by conditions is,

$$\underline{\boldsymbol{A}}\,\underline{\mathrm{dP}} + \underline{\boldsymbol{B}}\,\underline{\mathbf{v}} + \underline{w} = \underline{0} \tag{10}$$

where $\underline{A}$ and $\underline{B}$ denotes the Jacobian matrixes constituted by the EOP and observations (look angles), respectively, and $\underline{w}$ is the miscloser vector. The unknowns ($\underline{dP}$) are estimated as

$$\underline{\mathrm{dP}} = (\underline{\boldsymbol{A}}^{\mathrm{T}}(\underline{\boldsymbol{B}\boldsymbol{B}}^{\mathrm{T}})^{-1}\underline{\boldsymbol{A}})^{-1}\underline{\boldsymbol{A}}^{\mathrm{T}}(\underline{\boldsymbol{B}\boldsymbol{B}}^{\mathrm{T}})^{-1}\,\underline{w} \tag{11}$$

and the residuals are estimated as

$$\underline{\mathbf{v}} = \underline{\boldsymbol{B}}^{\mathrm{T}}\left(\underline{\boldsymbol{B}\boldsymbol{B}}^{\mathrm{T}}\right)^{-1}(\underline{\boldsymbol{A}}\underline{\mathrm{dP}} + \underline{w}) \tag{12}$$

Following the estimation of adjusted observation

$$\bar{\underline{\mathbf{L}}} = \underline{\boldsymbol{L}} + \underline{\mathbf{v}} \tag{13}$$

and adjusted parameters

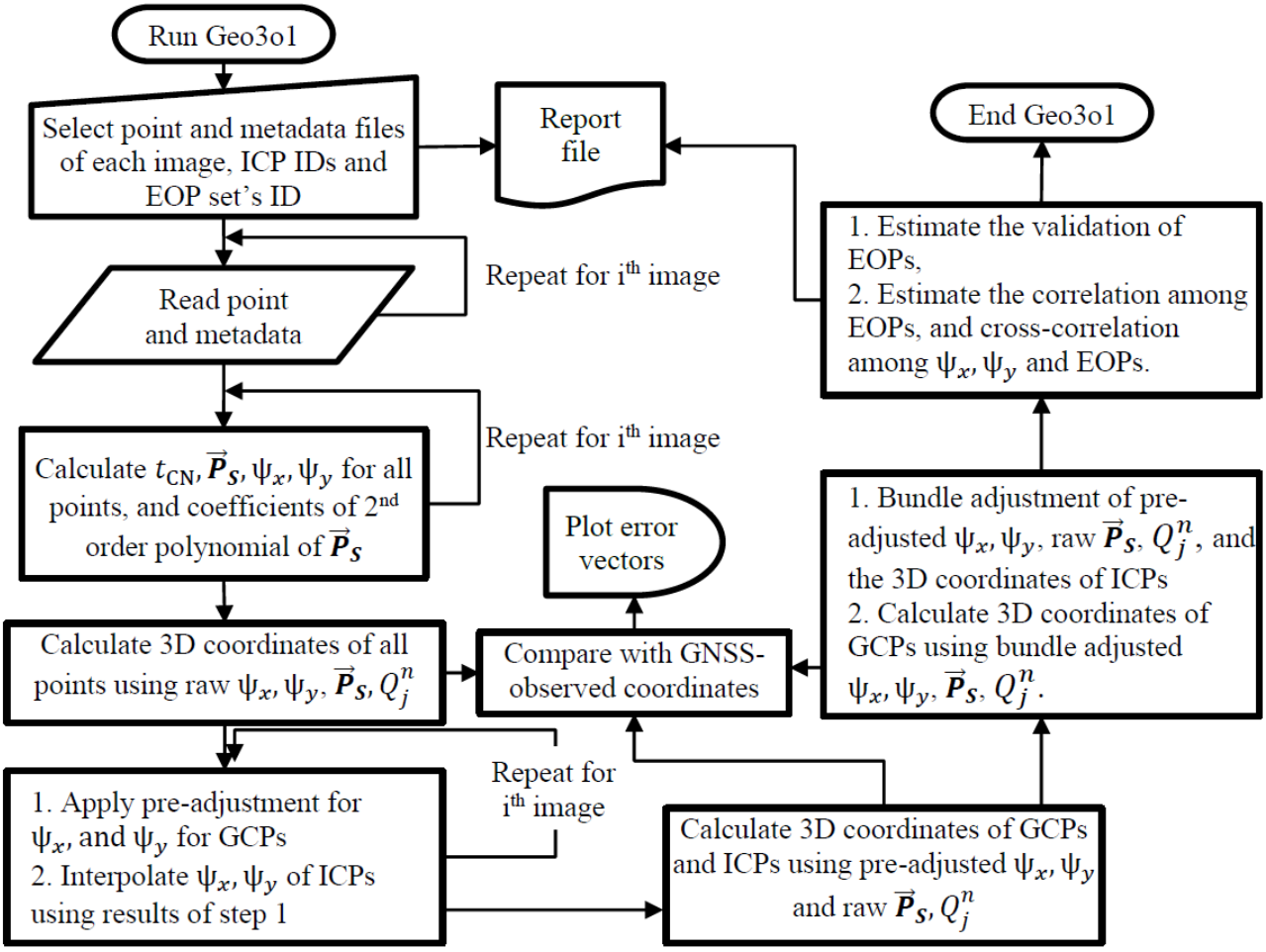

Fig. 1 – Workflow of Geo3o1 [20].

$$\underline{\overline{\boldsymbol{P}}} = \underline{P}\big|_0 + \underline{\mathrm{dp}} \tag{14}$$

The condition $\mathrm{F}(\underline{\overline{\mathrm{P}}}, \underline{\overline{\mathrm{L}}}) \triangleq 0$ must be confirmed. The $\underline{\boldsymbol{P}}$ are

$$\underline{\boldsymbol{P}} = \begin{bmatrix} t_{\mathrm{ref}}\ t_{\mathrm{period}}\ t_{\mathrm{offset}}\ t_{\mathrm{scale}}\ X_{S_0}\ \dot{X}_S\ \ddot{X}_S\ Y_{S_0}\ \dot{Y}_S\ \ddot{Y}_S\ Z_{S_0}\ \dot{Z}_S\ \ddot{Z}_S \ldots \\ Q_{0_0}\ \dot{Q}_0\ \ddot{Q}_0\ \dddot{Q}_0\ Q_{1_0}\ \dot{Q}_1\ \ddot{Q}_1\ \dddot{Q}_1\ Q_{2_0}\ \dot{Q}_2\ \ddot{Q}_2\ \dddot{Q}_2\ Q_{3_0}\ \dot{Q}_3\ \ddot{Q}_3\ \dddot{Q}_3\ \mathrm{X}_{ICP}\ \mathrm{Y}_{ICP}\ \mathrm{Z}_{ICP} \end{bmatrix}^{\mathrm{T}} \tag{15}$$

where $X_S = X_{S_0} + \dot{X}_S(x - x_{ref}) + \ddot{X}_S(x - x_{ref})^2$, and is valid for Y_S and Z_S.

The adjustment process of this article was completed in two steps. At the first step, the look angles (ψ_x, ψ_y) were adjusted in pre-adjustment step for each image of stereopair, and then these pre-adjusted look angles and raw EOPs are taken into the bundle adjustment step.

The EOPs ($\underline{P}$) are assumed constant, and only the look angles $\underline{L}$ of ground control points (GCPs) are adjusted. In this case, $\underline{\mathrm{dP}} = 0 \rightarrow \underline{\boldsymbol{A}}\,\underline{\mathrm{dP}} = \underline{0}$, and the functional model is formulated as $\underline{\boldsymbol{B}}\,\underline{\mathbf{v}} + \underline{w} = \underline{0}$. The look angles of ICPs are interpolated using these pre-adjusted look angles of GCPs as following:

$$\boldsymbol{A}_{\psi_i} = [1\ (x - x_{\mathrm{ref}})_i\ (y - y_{\mathrm{ref}})_i], \psi \in (\psi_x, \psi_y) \tag{16}$$

$$b_{\psi_i} = [\psi_i] \tag{17}$$

$$\underline{c}_\psi = (\underline{\boldsymbol{A}}_\psi^{\mathrm{T}}\underline{\boldsymbol{A}}_\psi)^{-1}\underline{\boldsymbol{A}}_\psi^{\mathrm{T}}\underline{b}_\psi \tag{18}$$

$$\psi_{ICP} = \underline{c}_\psi^{\mathrm{T}}[1\ (x - x_{ref})_{ICP}\ (y - y_{ref})_{ICP}]^{\mathrm{T}} \tag{19}$$

The functional model of bundle adjustment is the expanded form of Eq. (10) consisting of more than one image. In our case, the look angles, EOPs of two images of a stereopair, and 3D ground coordinates of ICPs were bundle adjusted. So, the accuracy was calculated by the difference of estimated coordinates (using adjusted look angles and EOPs) by the bundle adjustment and measured coordinates (by field survey) as

$$m_X = \pm\sqrt{\frac{[\Delta X \Delta X]}{p}}, \qquad m_Y = \pm\sqrt{\frac{[\Delta Y \Delta Y]}{p}}, \qquad m_Z = \pm\sqrt{\frac{[\Delta Z \Delta Z]}{p}} \tag{20}$$

where $\Delta X = \overline{\mathrm{X}}_{\mathrm{estimated}} - \mathrm{X}_{\mathrm{meausured}}$, and p is the number of GCP/ICPs.

In sensor-dependent orientation, correlation among the EOPs and between EOPs and IOPs should be investigated. In this case the correlation is formulated as following:

$$\underline{Q}_{dpdp} = (\underline{\boldsymbol{A}}^{\mathrm{T}}(\underline{\boldsymbol{B}\boldsymbol{B}}^{\mathrm{T}})^{-1}\underline{\boldsymbol{A}})^{\mathrm{T}} \tag{21}$$

$$r_{dP_1 dP_2} = \frac{q_{dP_1 dP_2}}{\sqrt{q_{dP_1 dP_2} q_{dP_1 dP_2}}} \tag{22}$$

where $\underline{Q}_{dpdp}$ denotes auto-cofactor matrix consisting of $q_{dP_1 dP_2}$, and $r_{dP_1 dP_2}$ is the correlation among two unknowns of parameters P_1 and P_2. The possible correlation among the IOPs and EOPs can be estimated as following:

$$\underline{Q}_{\psi dp} = -\underline{\boldsymbol{B}}^{\mathbf{T}}\left(\underline{\boldsymbol{B}\boldsymbol{B}}^{\mathbf{T}}\right)^{-1}\underline{\boldsymbol{A}}\,\underline{\boldsymbol{A}}^{\mathbf{T}}(\underline{\boldsymbol{B}\boldsymbol{B}}^{\mathbf{T}})^{-1}\underline{\boldsymbol{A}} \tag{23}$$

$$r_{\psi dp} = \frac{q_{\psi dp}}{\sqrt{q_{\psi dp}}} \tag{24}$$

where $\underline{Q}_{\psi dp}$ is cross-cofactor matrix, and $r_{\psi dp}$ is the correlation among observations (IOPs) and unknowns (EOPs). Statistical validation of the parameters is also analysed as following.

$$m_0 = \pm\sqrt{\frac{\mathbf{v}\mathbf{v}^{\mathbf{T}}}{n-u}} \tag{25}$$

$$T = \frac{|P_j|}{m_{dP_1}} \tag{26}$$

where m_0 and m_{dP_1} are root mean square error of unit weight and of parameters, respectively, and t is test value which must be greater than $t_{\alpha/2,f}$ for a valid parameter, where $\frac{\alpha}{2} = 0.025$ and $f = n - u$ is degree of freedom.

3. IMAGES, DATA, AND TEST SITE

The panchromatic images used in this article were dated November 1st, 2018, acquired in tri-stereo mode (Fig. 2). The geometric resolution varied from 0.51 m to 0.68 m causing the off-nadir acquisition. Their processing level was 2A corresponding to the *primary* product of Pléiades 1A/1B/Neo, and SPOT 6&7. The imaging configuration is illustrated in Fig. 2, and the details of the stereo imaging configurations and the values obtained from the metadata files of the Göktürk-1 images are given in Table 1.

The test site covers the Zonguldak city centre and its surroundings (Türkiye). This area is very suitable for the research on remotely sensed images since it is located on a mountainous and extremely undulated topography with various land covers. Zonguldak city centre is also located on this undulating mountainous area settled along the Black Sea. Various type of airborne and spaceborne remotely sensed optical and microwave images were examined on this test site since 2000s. The height ranges from sea level to 925 m. Totally 59 points surveyed by GNSS (Global Navigation Satellite Systems) observations in real time kinematic mode were used supplying the 3D accuracy ranging from ±4 mm to ±283 mm [15, 22], and most were under

the accuracy limit suggested by [23]. Most of these points were collected on the centre of symmetric objects such as narrow road intersections, roundabouts, small bridges etc. on the bare ground. All points were distributed as homogeneously as possible in both horizontal and vertical planes. The point distribution is dense at the urban areas comparing with the rural and forest areas. Fig. 3 presents the various GCP/ICP distributions.

Table 1

Specifications of stereo imaging configurations [14, 15].

Stereo-pairs	Time difference of imaging (sec)	Base (km)	B/H	Converge angle (°)
82902-83118	48	364.7	0.53	27.35
83118-83350	55	417.8	0.61	31.51
82902-83350	103	782.5	1.14	58.86

a) Zonguldak province

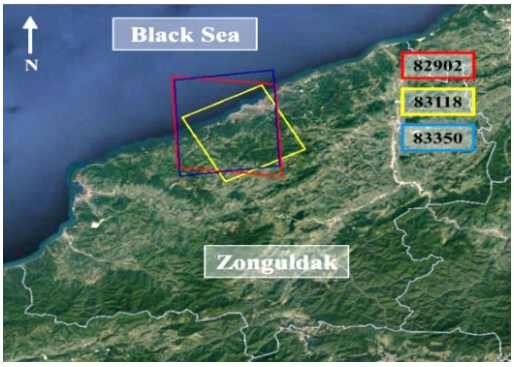

b) Imaged area on Zonguldak test site.

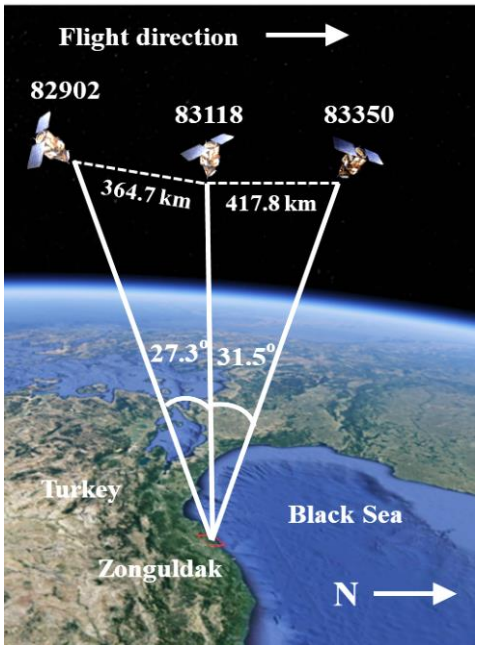

c) Imaging configuration (background: Google Earth).

Fig. 2 – Location of test site and imaging configuration.[15].

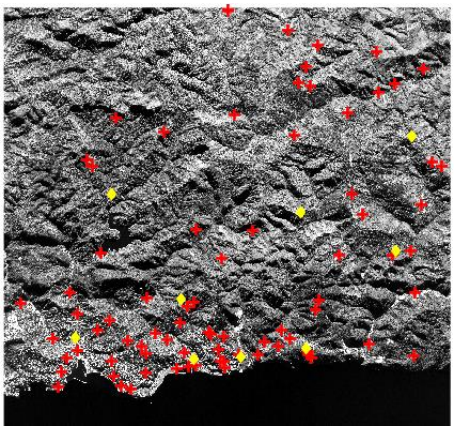

Point set 1 (#GCP=50, #ICP=9)

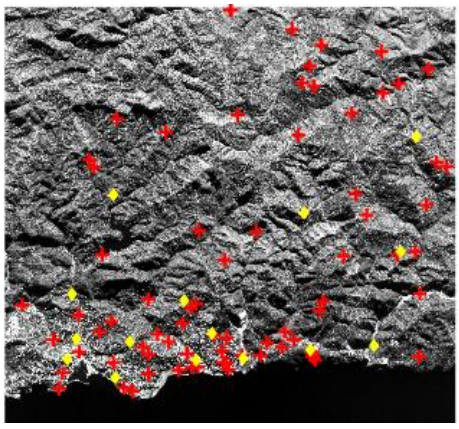

Point set 2 (#GCP=44, #ICP=15)

Fig. 3 – Point sets. +: GCP, ◊: ICP [15].

4. RESULTS

This section was constituted in three parts. At first, the accuracy of direct georeferencing was presented. Then, the results of adjustment process and limitation of research were presented, respectively.

4.1. Accuracy by direct georeferencing

Direct georeferencing accuracy is an initial metric showing the georeferencing potential of a remote sensing satellite, especially when the ground truth is not available. This metric illustrates the geometric quality of imaging system and the instruments supplying the orientation parameters. Direct georeferencing accuracy was estimated by using the raw look angles and EOPs traditionally called the interior and exterior orientation parameters, respectively. According to [7], Telespazio warranted the direct georeferencing accuracy ± 10 m without GCPs for the imaging up to 10° incidence angle. This accuracy was estimated as ±12.62 m, ±8.21 m, ±6.40 m and ±7.96 m for stereo pairs 82902-83118, 82902-83350, 83118-83350 and tri-stereo, respectively (Table 2). The vector plot of residuals had a systematic pattern as expected (Fig. 4). These results almost supported the desired direct georeferencing accuracy. However, neither the stereopair 82902-83350 with highest *B*/*H* nor the tri-stereo set achieved the highest accuracy for direct georeferencing.

Table 2

Results of 3D direct georeferencing accuracy ($\pm m$) [15]

Stereopair ID	m_x	m_y	m_z	$m_0=\pm\sqrt{m_x^2+m_y^2+m_z^2}$
82902-83118	2.36	10.35	6.83	12.62
82902-83350	3.30	5.50	5.13	8.21
83118-83350	4.35	4.17	2.16	6.40
Tri-stereo	2.27	6.63	3.79	7.96

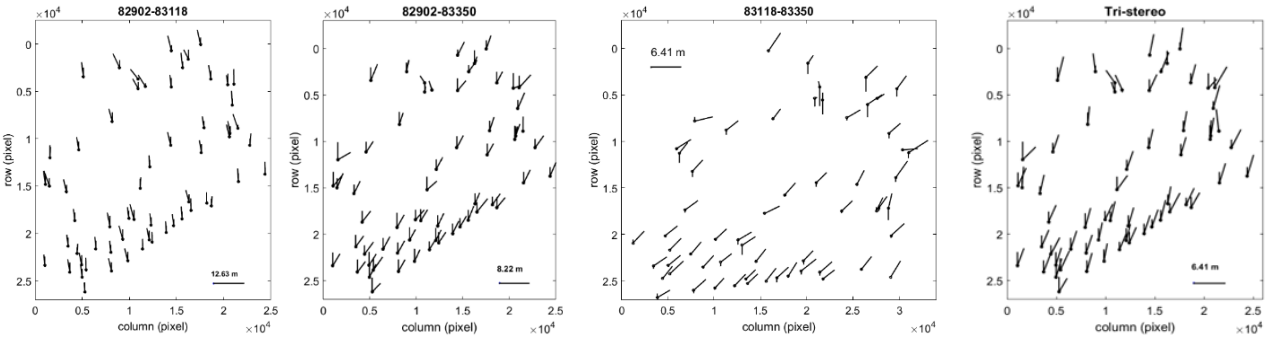

Fig, 4 – Plot of residual errors at all points after direct georeferencing (diagonal: XY, up-down: Z).

4.2. Accuracy by adjustment

Although the direct georeferencing of an imaging sensor gives an idea to the users if the ground truth is unavailable, the adjustment process is widely applied to get more accurate georeferenced products such as orthoimage or digital elevation model. As mentioned by [15, 20, 21] the adjustment process was handled in two stages. At the first stage, the raw look angles of GCPs were adjusted while the raw EOPs were assumed constant, for each images individually. Then, the look angles of ICPs and ground coordinates of both GCPs and ICPs were estimated and compared by their ground truth. The results of pre-adjustment as presented in the Table 3. The accuracies were under-millimetre level at GCPs and ±1 GSD (~50 cm) at ICPs. The accuracy in ICPs complied with the standard defined by [23, 24, 25], which the ICP accuracy should be less than GSD. The highest accuracy was achieved by both stereopair 82902-83350 with highest B/H and the tri-stereo set since the 3D coordinates with high accuracy were naturally estimated by highest B/H. Figure 5 shows the residual errors illustrating the random pattern. Among them, only the stereopair 83118-83350 resulted the higher error in *Z* direction than *X* and *Y* directions.

Bundle adjustment was applied following the pre-adjustment stage. In this case, three EOP sets were chosen, *i.e.* $\underline{\boldsymbol{P_1}} = t_{\text{ref}}$, $\underline{\boldsymbol{P_2}} = [X_{U_0}\ Y_{U_0}\ Z_{U_0}]^{\text{T}}$ and $\underline{\boldsymbol{P_3}} = [Q_{0_0}\ Q_{1_0}\ Q_{2_0}\ Q_{3_0}]^{\text{T}}$. The motivation of setting $\underline{\boldsymbol{P_1}}$ was that all other EOPs (coefficients of $\vec{\boldsymbol{P}}_{\boldsymbol{S}}$ and elements of $\underline{\boldsymbol{R}}$) were already estimated using the t_{ref}, t_{period}, and t_{offset}. Two other motivations were to reduce the number of parameters in the adjustment [26], and the dominating error source was the look angles in our case. Table 3 was also presented the findings of bundle adjustment. Although there is no difference between both adjustment types for ICPs, a little but negligible difference (from 10^{-4} m to 10^{-3} m) occurred at GCPs caused by the matrix structure and inversion. However, the accuracies at GCPs did not exceed millimetre level. Such kind of ultra-high accuracy could be estimated when a sensor dependent orientation model and the accurate auxiliary data such as metadata of image and GNSS surveyed points are available [20, 21, 27, 28, 29]. The accuracy differences at GCPs depending various EOP sets (i.e. $\underline{\boldsymbol{P_1}}$, $\underline{\boldsymbol{P_2}}$ and $\underline{\boldsymbol{P_3}}$) could be negligible since they are 10^{-3} m level. Instead, the real georeferencing accuracy was explored by the ICPs. Although the number of GCPs decreased from 50 to 44, the accuracy at ICPs moderately increased. The residuals at GCPs showed non-systematic pattern after pre-adjustment (Fig. 5) while they were systematic after bundle adjustment, depending on the EOP sets (Fig. 6). For instance, $\underline{\boldsymbol{P_2}}$ and $\underline{\boldsymbol{P_3}}$ resulted various effects at the upper (geographically south) and bottom (geographically north) sides of images. A sample has been presented by Fig. 7 using point set 1 for stereopair 82902-83118.

The validation of EOPs was also analysed resulting they were invalid, *i.e.* they could be used with their raw values in adjustment process. The correlation among EOPs and cross-correlation between EOPs and look angles were also investigated. The correlation among EOPs varied between ±1.00, *i.e.* the negative and positive correlations with highest level were occurred. Despite this unexpected result, the ill-posedness was not observed. The cross-correlation among the look angles and EOPs was negligible, for instance this value was between –0.15 and +0.10 for the EOP set $\underline{\boldsymbol{P_3}}$ in the GCP/ICP set I.

Table 3

Results of 3D georeferencing accuracy (± meter) [15].

Stereopair ID	Point		Pre-adjustment ($\times 10^{-4}$ for GCPs)			Bundle adjustment ($\times 10^{-3}$ for GCPs)								
						t_{referans}			$X_{U_0}\ Y_{U_0}\ Z_{U_0}$			$Q_{0_0}, Q_{1_0}, Q_{2_0}, Q_{3_0}$		
	Set ID	GCP ICP	m_x	m_y	m_z	m_x	m_y	m_z	m_x	m_y	m_z	m_x	m_y	m_z
82902 83118	I	50	5.62	6.67	4.81	2.07	2.31	4.87	7.85	8.29	6.44	8.78	3.22	9.40
		9	0.71	0.53	0.99	0.70	0.53	0.99	0.70	0.53	0.99	0.70	0.52	0.99
	II	44	5.90	7.00	5.04	4.73	5.32	11.1	21.3	22.9	17.4	24.2	3.70	23.9
		15	0.72	0.58	0.85	0.76	0.52	0.86	0.75	0.52	0.86	0.75	0.52	0.86
82902 83350	I	50	0.83	1.56	3.14	5.88	7.51	9.46	7.93	9.44	12.5	11.90	14.78	18.93
		9	0.57	0.56	0.89	0.57	0.56	0.90	0.57	0.56	0.90	0.57	0.57	0.90
	II	44	0.84	1.58	3.26	9.77	12.50	15.7	13.7	16.3	21.6	21.25	25.85	33.67
		15	0.57	0.47	0.77	0.57	0.48	0.77	0.57	0.48	0.78	0.57	0.48	0.77
83118 83350	I	50	1.71	2.04	5.93	0.12	3.16	0.63	3.57	7.03	11.62	3.10	6.49	5.62
		9	0.54	0.58	0.81	0.54	0.58	0.81	0.54	0.58	0.82	0.54	0.58	0.82
	II	44	1.78	2.12	6.18	0.09	2.30	0.43	3.54	6.98	11.70	3.30	6.88	6.42
		15	0.52	0.50	0.79	0.52	0.50	0.79	0.52	0.50	0.80	0.52	0.50	0.80
Tri-stereo	I	50	1.65	2.31	2.48	15.3	7.65	5.80	9.14	11.6	12.2	14.13	14.81	18.68
		9	0.54	0.47	0.84	0.54	0.49	0.85	0.53	0.49	0.85	0.53	0.50	0.85
	II	44	1.72	2.38	2.53	19.7	9.29	14.65	15.3	16.4	22.9	25.31	22.69	35.87
		15	0.55	0.41	0.73	0.53	0.42	0.74	0.53	0.42	0.75	0.53	0.42	0.74

4.3. Limitation

The major limitation of this research was the estimating the look angles of ICPs interpolated from the pre-adjusted look angles of GCPs. The challenge of this interpolation is to precisely estimate ψ_y. Although this parameter is calculated by a polynomial function, only one coefficient (0^{th} order) is given by the metadata file. Following the pre-adjustment process, this parameter was varied for each GCPs, and it was not a function of *y* axis.

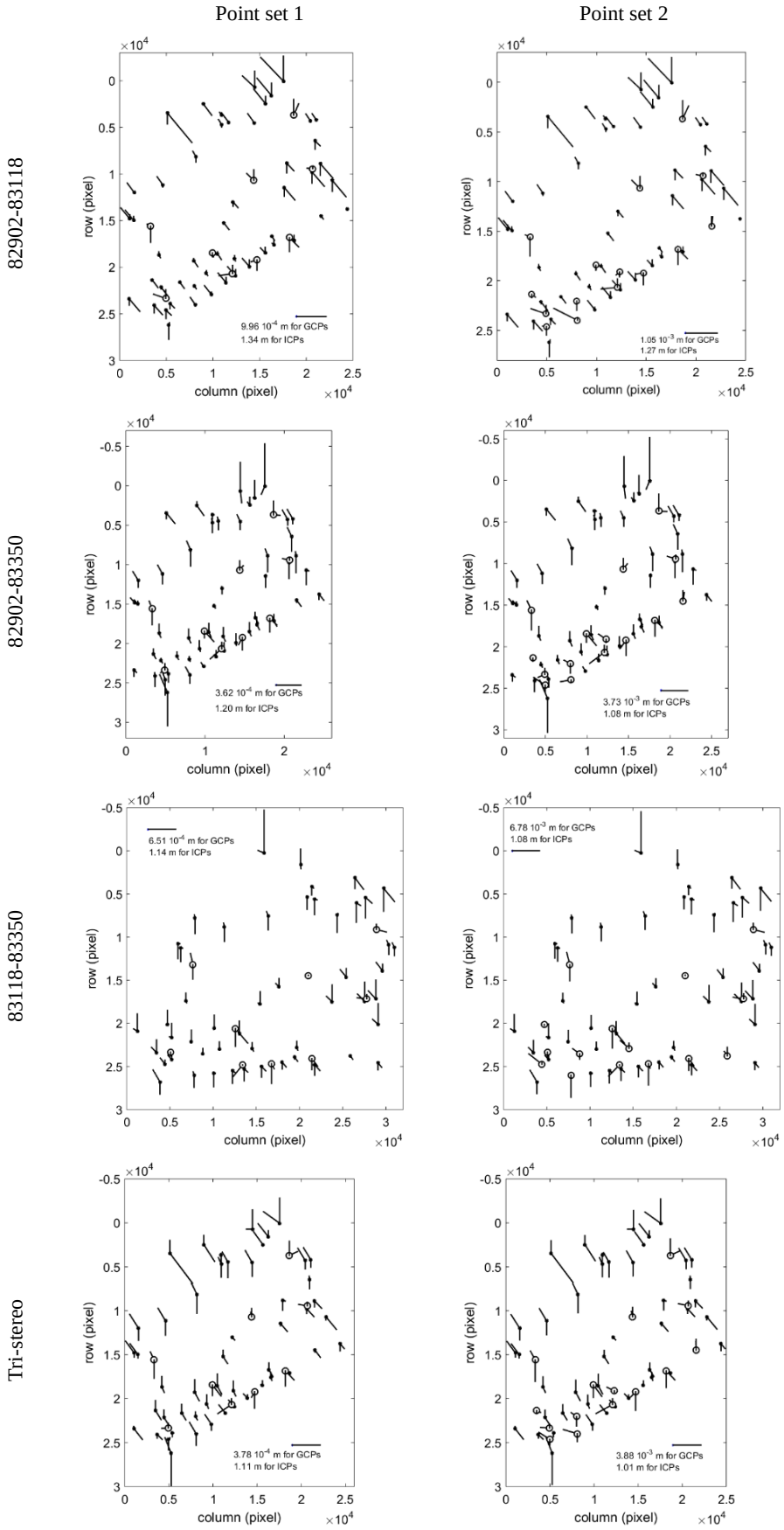

Fig. 5 – Plot of residual errors at GCPs (•) and at ICPs (°) after pre-adjustment.

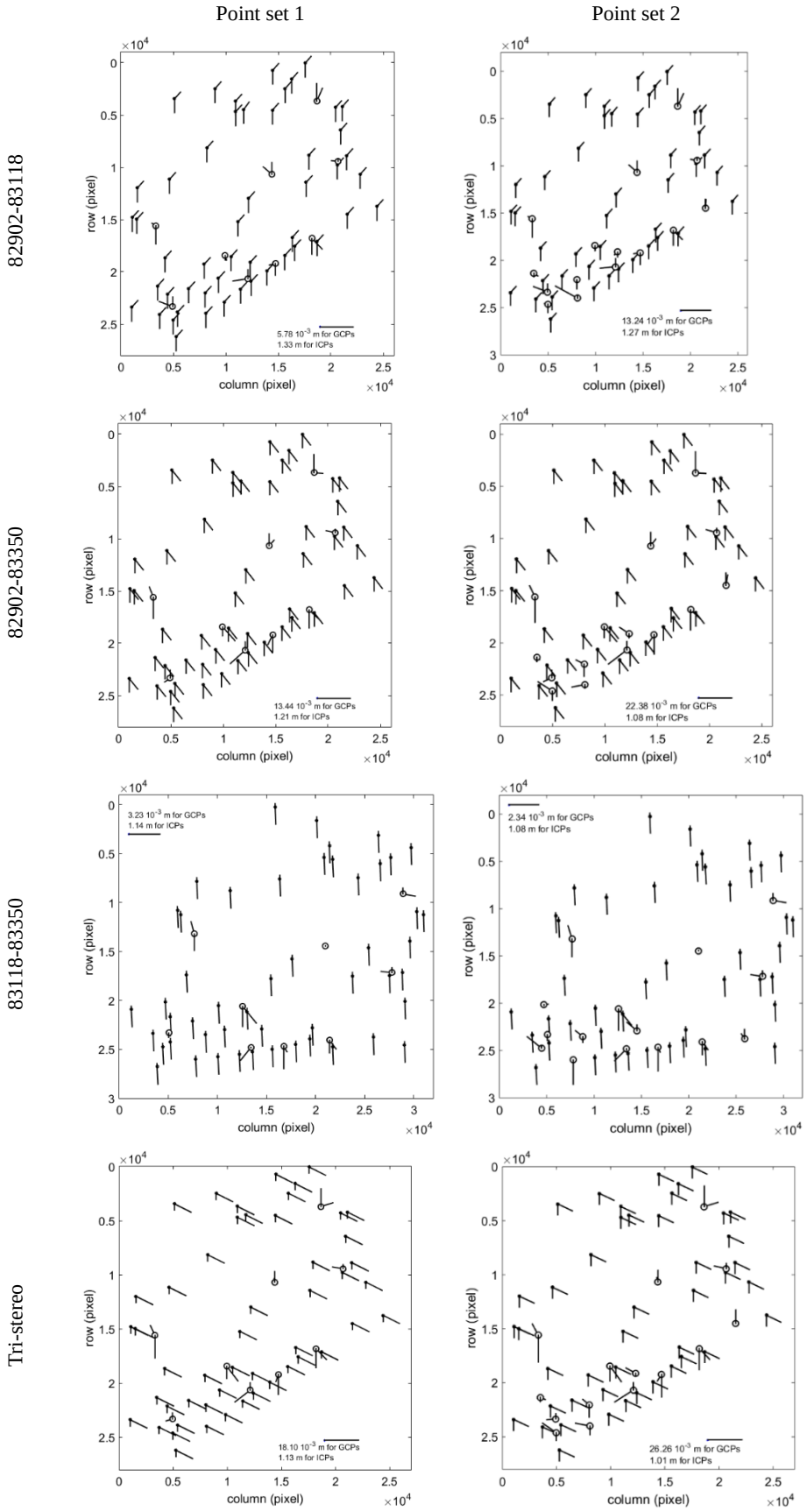

Fig. 6 – Plot of residual errors at GCPs (•) and at ICPs (°) after bundle adjustment.

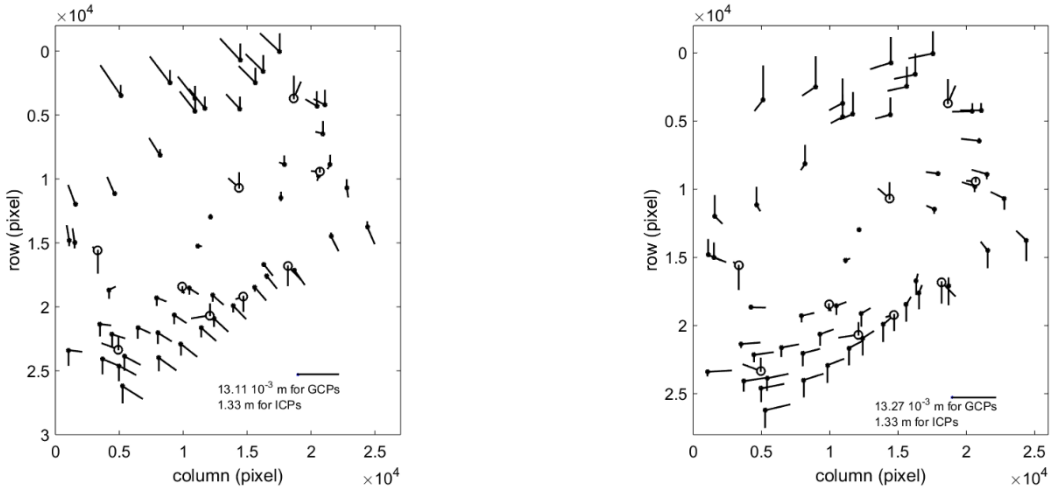

Fig. 7 – Plot of residual errors at GCPs (•) and at ICPs (°) of point set 1 after bundle adjustment for $\underline{\boldsymbol{P}}_2$ and $\underline{\boldsymbol{P}}_3$.

This means a proper interpolation method was required for this parameter. Although the various types of methods based on surface-modelling or triangulation were implemented, the method suggested by [20] resulted the best. Nevertheless, this method depends on the point distribution, i.e. the points must be evenly distributed in planimetry, and the ICPs must be surrounded by the GCPs. The alternate interpolation methods or functional models in adjustment could be investigated in the future.

5. CONCLUSIONS

This research presented the 3D georeferencing accuracy of stereo panchromatic level 2A images of Göktürk-1, the first sub meter optical remote sensing satellite of Türkiye, using its sensor dependent orientation model. Besides, the efficiency of its interior and exterior orientation parameters on the georeferencing accuracy was also investigated. The research was conducted in an undulating mountainous topography (Zonguldak, Türkiye) with two GCP/ICP sets. The findings showed us that the Göktürk-1 sufficed the direct georeferencing accuracy of ±10 m up to 10° inclination angle, aimed by the prime conductor, Telespazio. This accuracy was improved by the adjustment process in two stages, i.e. pre- and bundle adjustment. Pre-adjustment stage adjusted only the look angles (interior orientation parameters) of each image individually, and reached sub-millimeter accuracy at GCPs, but not for ICPs. Although the accuracy at ICPs conformed to the national and international standards, they were relatively lower than the accuracy at the GCPs, as result of estimating their look angles from the ψ_y of GCPs. Bundle adjustment was applied by varied sets of EOPs as unknown, and desired accuracy could be reached for each set. Although the correlation among EOPs varied ±1, the ill-posedness did not arise, and the cross correlation between interior and exterior orientation models were negligible level. The further evaluation could be extended in different test sites solving the challenge mentioned in the limitation section.

ACKNOWLEDGEMENTS

The authors would like to thank to Turkish Air Forces for supporting the images, and to TÜBİTAK (Grant Number: 114Y380) and to Zonguldak Bülent Ecevit University Scientific Research Projects Fund (Grant Number: 2014-47912266-01) since the points used in this research were already collected by these projects, and to Prof. Dr. Bahattin Erdoğan for his contribution to the look angle estimation. This research was derived from the first author's PhD thesis and subjected in the research protocol between Zonguldak Bülent Ecevit University and General Directorate of Mapping.

REFERENCES

[1] Telespazio. Göktürk-1, https://www.telespazio.com/en/programmes/gokturk [accessed 14.02.2022].

[2] Polat HC, Atak VO, Kocabıçak İE, Gürçay E, Gültekin FG, Yanteri EE. Satellite imagery calibration and quality assessment tests: GÖKTÜRK-1 Case Study. In: 2019 9th International Conference on Recent Advances in Space Technologies (RAST). June 11–14, 2019.

[3] Gültekin FG, Atak VO, Ayaz ME, Arı M. Geometric accuracy in satellite imagery: Test methods & Göktürk-1 performance evaluation. In: 2019 9th International Conference on Recent Advances in Space Technologies (RAST). June 11–14, 2019.

[4] Boccardo P, Sandu C, Ajmar A, Perez F. Digital surface models extraction by Göktürk-1 satellite stereo pairs. In: 2019 9th International Conference on Recent Advances in Space Technologies (RAST). June 11–14, 2019.

[5] Yavaş G, Sezer A. GÖKTÜRK-1 satellite system level radiated emission and radiated susceptibility tests. In: 2019 9th International Conference on Recent Advances in Space Technologies (RAST). June 11–14, 2019.

[6] Tarçın AÇ, Poyraz Ü, Bayramoğlu M, Şahin DÖ, Yalçınkaya E, Çelebioğlu O. GÖKTÜRK-1 satellite propulsion subsystem design, integration, test and launch campaign activities. In: 2019 9th International Conference on Recent Advances in Space Technologies (RAST). June 11–14, 2019.

[7] Arasan G, Yılmaz A, Firat O, Avşar E, Güner H, Ayğan K, Yüce D. Accuracy assessment of GÖKTÜRK-1 satellite imagery. International Journal of Engineering and Geosciences. 2020; 5(3): 160–168. DOI: 10.26833/ijeg.650899.

[8] Ravanelli R, Lastilla L, Crespi M. Orthoimage generation by GÖKTÜRK-1: A test case in Rome. In: 2019 9th International Conference on Recent Advances in Space Technologies (RAST). June 11–14, 2019.

[9] Ottaviano M, Sertel E, Marchetti M. Turkish satellite Göktürk-1 at work: Applications for artificial, natural and semi-natural resources, mapping and inventory. In: 2019 9th International Conference on Recent Advances in Space Technologies (RAST). June 11–14, 2019.

[10] Ünal A, Yıldız F. Göktürk-1 Uydu Görüntülerinin Pankeskinleştirme Performansının İncelenmesi. Geomatik. 2022; 6(2): 148–64. DOI: 10.29128/geomatik.731816.

[11] Çetin M, Köksal E. Piksel ve Nesne Tabanlı Sınıflandırma Metodları Kullanılarak Göktürk 1 Uydu Görüntülerinin Değerlendirilmesi. In: EFIS Zonguldak. 2020.

[12] Aytekin G, Topan H, Elkar Y.E, Kişi M, Erişik O. 2D orientation accuracy of Göktürk-1 panchromatic imagery. In: 2019 9th International Conference on Recent Advances in Space Technologies (RAST), İstanbul, Turkey. June 11–14, 2019.

[13] Aytekin G, Topan H. Göktürk-1 Uydu Görüntülerinin Konum Doğruluğunun Algılayıcıya Bağımlı Yöneltme Modeli ile Belirlenmesi. In: XI. Türkiye Ulusal Fotogrametri ve Uzaktan Algılama Birliği (TUFUAB) Teknik Sempozyumu. edited by Murat Yakar. Mersin, Türkiye; 2022a.

[14] Aytekin G, Topan H. Üçlü Bindirmeli Göktürk-1 Uydu Görüntülerinin Konum Doğruluğunun Zonguldak Test Alanında Algılayıcıya Bağımlı Yöneltme Modeli ile Belirlenmesi. Harita Dergisi. 2022b; 168; 13–27.

[15] Aytekin G. Algılayıcıya Bağımlı Yöneltme Modeli ile Üçlü Bindirmeli Görüntülerin Konum Doğruluğunun Belirlenmesi [Ph.D. thesis], Zonguldak Bülent Ecevit Üniversitesi; 2023.

[16] Airbus Defence and Space. Pléiades Imagery User Guide. V 2.0 ed. 2012.

[17] Airbus Defence and Space. SPOT 6 & SPOT 7 Imagery User Guide. 2013.

[18] Airbus Defence and Space. Pléiades Neo User Guide. 2022.

[19] Riazanoff S. SPOT 123-4-5 geometry handbook. France: Spot Image; 2004.

[20] Topan H. Geo3o1: A tool for 3D georeferencing accuracy assessment of tri-stereo images by state-of-the-art sensor dependent orientation model. Journal of Applied Remote Sensing 2022; 16(4): 047502. DOI: 10.1117/1.JRS.16.047502.

[21] Topan H. First experience of 3D georeferencing accuracy assessment of SPOT 6 stereo panchromatic primary images by sensor-dependent orientation model. Remote Sensing Letters. 2023; 14(12): 1294–1302. DOI:10.1080/2150704X.2023.2285736.

[22] Topan H, Jacobsen K, Cam A, Ozendi M, Oruç M, Bakioğlu OB, Bayık Ç, Taşkanat T. Comprehensive evaluation of Pléiades-1A bundle images for geospatial applications. Arabian Journal of Geosciences. 2019; 12: 223. DOI: 10.1007/s12517-019-4353-9.

[23] Kapnias D, Milenov P, Kay S. Guidelines for best practice and quality checking of ortho imagery. European Commission, Joint Research Centre, Institute for the Protection and Security of the Citizen; 2008.

[24] ASPRS. ASPRS positional accuracy standards for digital geospatial data. Photogrammetric Engineering & Remote Sensing. 2015; 81(3): A1–A26. DOI: 10.14358/pers.81.3. a1-a26.

[25] BÖHHBÜY. Büyük Ölçekli Harita ve Harita Bilgileri Üretim Yönetmeliği. 2018.

[26] Ghilani C, Wolf PR. Adjustment computations. 4th ed. John Wiley & Sons, Inc.; 2006.

[27] Leprince S, Barbot S, Ayoub F, Avouac JP. Automatic and precise orthorectification, coregistration, and subpixel correlation of satellite images, application to ground deformation measurements. IEEE Transactions on Geoscience and Remote Sensing. 2007; 45(6): 1529–1558. DOI: 10.1109/Tgrs.2006.888937.

[28] Leprince S, Muse P, Avouac JP. In-flight CCD distortion calibration for pushbroom satellites based on subpixel correlation. IEEE Transactions on Geoscience and Remote Sensing. 2008; 46(9): 2675–2683. DOI: 10.1109/Tgrs.2008.918649.

[29] Topan H, Maktav D. Efficiency of orientation parameters on georeferencing accuracy of SPOT-5 HRG level-1A stereoimages. IEEE Transactions on Geoscience and Remote Sensing. 2014; 52(6): 3683–3694. DOI: 10.1007/s12524-013-0273-4.

Received April 1, 2024